

# Visualization of microscale phase displacement processes in retention and outflow experiments: Nonuniqueness of unsaturated flow properties

Annette P. Mortensen

Department of Hydrodynamics and Water Resources, Technical University of Denmark, Lyngby, Denmark

Robert J. Glass

Flow Visualization and Processes Laboratory, Sandia National Laboratories, Albuquerque, New Mexico

Karl Hollenbeck<sup>1</sup> and Karsten H. Jensen

Department of Hydrodynamics and Water Resources, Technical University of Denmark, Lyngby, Denmark

**Abstract.** Methods to determine unsaturated hydraulic properties can exhibit random and nonunique behavior. We assess the causes for these behaviors by visualizing microscale phase displacement processes that occur during equilibrium retention and transient outflow experiments. For both types of experiments we observe the drainage process to be composed of a mixture of fast air fingering and slower air back-filling. The influence of each of these microscale processes is controlled by a combination of the size and the speed of the applied boundary step, the initial saturation and its structure, and small-scale heterogeneities. Because the mixture of these microscale processes yields macroscale effective behavior, measured unsaturated flow properties are also a function of these controls. Such results suggest limitations on the current definitions and uniqueness of unsaturated hydraulic properties.

## 1. Introduction

Researchers and practitioners alike have measured unsaturated hydraulic properties of granular porous media since *Buckingham* [1907]. Methods used have evolved from original hydrostatic and steady state methods [e.g., *Klute*, 1986; *Corey*, 1985] to more recent transient methods where nonlinear inversion must be employed (see review by *Hopmans and Šimůnek* [1999]). However, reproducibility is often difficult to achieve either across different but essentially identical samples of the same granular material [e.g., *van Dam et al.*, 1994] or in a single sample with the same measurements repeated sequentially in time [e.g., *Hollenbeck and Jensen*, 1998]. Also, one finds additional discrepancies between properties measured with different methods [e.g., *Stolte et al.*, 1994] and at different scales [e.g., *Kasteel et al.*, 1999]. Many possible explanations for this experimental response exist such as slight differences in equilibration time, initial conditions, internal sample heterogeneity, contact between sample and boundary conditions, microbial growth, changing fluid-fluid-solid contact angle, swelling or consolidation of the sample, disturbances of the experiment while making measurements, etc. Because of the myriad of possible explanations, fundamental examination of hydraulic properties themselves is important.

In a recent consideration of hydraulic property inversion,

*Hollenbeck and Jensen* [1998] presented a careful study of transient single and multistep outflow in a single sample. Their results showed that at low suctions, significant randomness in outflow response occurred for identical (or nearly identical) effective initial and boundary conditions. For high suctions, good repeatability was found but nearly identical outflow response occurred for different boundary conditions where significant differences were predicted. An accompanying error analysis suggested that the discrepancies noted were not due to measurement errors, and further, it was concluded that the observed outflow variability could not be described by the Richards equation using standard parametric relations for hydraulic properties. Because only sample-scale effective behavior was observed by the authors, the causes for this mismatch could only be speculated.

Our interest here is in the causes of discrepancies in sample-scale effective behavior between repeat experiments, between different types of experiments, boundary or initial conditions, and, most importantly, between experimental behavior and that predicted or implied by standard continuum conceptual models for unsaturated flow in porous media. We present the results of a series of experiments specifically designed to visualize quantitatively the active underlying microscale processes in simple equilibrium retention experiments and transient outflow experiments. Our experiments illustrate the interaction between slight subsample heterogeneity, imposed boundary pressures or fluxes, and initial saturation and its structure to control the qualitative and quantitative behavior of the microscale phase invasion process. Sample-scale effective behavior thus exhibits additional dependence that suggests limitations in the current definitions and uniqueness of unsaturated hydraulic properties.

<sup>1</sup>Now at DHI Water and Environment, Hørsholm, Denmark.

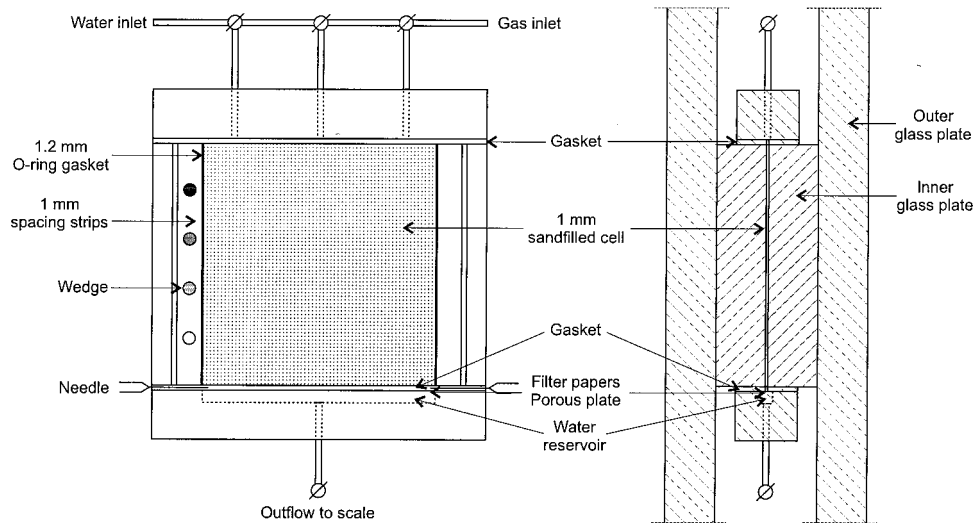


**Figure 1.** Schematic of the experimental setup showing (left) plan view and (right) cross section of the inner cell.

## 2. Experimental Design and Methods

We consider the standard experimental configuration where a gravity stabilized drainage process in a granular sample is measured at the system scale. The nonwetting phase (usually air) enters the system from the top, and the wetting phase (usually water) exits from the bottom through a porous plate. A differential phase pressure is imposed on the system by either increasing the pressure in the air relative to the water or decreasing the pressure of the water relative to the air. The range of differential phase pressures that can be applied are limited by the air entry pressure of the bottom porous plate. Two types of experiments are commonly conducted with this system. By imposing a series of small step changes in capillary pressure, such as lowering a hanging column of water connected to the porous plate and waiting until no more water leaves the system, equilibrium water retention curves are measured. Second, a single or series of larger boundary pressure steps can be imposed, and the outflow as a function of time measured and inverted to yield parameters for assumed water retention and relative permeability functions.

In order to explore microscale behavior within such experiments we designed our system so that quantitative visualization of the pore structure and saturation fields within the sample was possible as a function of time. This design allows us to evaluate the heterogeneity structure, the initial saturation fields, and the microscale processes active during the conduct of simple phase displacements. It also allows us to detect slight changes that could occur within the sample such as compaction, microbial growth, etc. For this purpose we chose to apply the charge-coupled device (CCD)-based two-dimensional light transmission technique of *Tidwell and Glass* [1994] as it has high spatial resolution ( $\sim$ pore scale), is rapid (an entire  $\sim 10^6$  point field can be measured in a fraction of a second), and can distinguish between small changes in saturation at each point in the field (high sensor signal-to-noise ratio). The technique can be applied to thin but extensive systems that transmit light and yield an image that integrates the saturation across the cell thickness at each point in the field. As we are interested in microscale behavior, we applied the technique using a small micromodel ( $10 \text{ cm} \times 10 \text{ cm} \times 0.1 \text{ cm}$  thick)

composed of an  $\sim 2$ – $4$  grain thick layer of rounded naturally occurring sand similar to that previously used by *Hollenbeck and Jensen* [1998]. This system yielded a spatial resolution in the plane of the cell that was approximately pore scale ( $0.1 \text{ mm}$ ) yet extensive ( $\sim 250$  grains wide and tall) while maintaining an average of 3–5 pores in thickness. Thus the system forms a thin three-dimensional (3-D) pore network that falls between standard single-pore wide etched micromodels [e.g., *Conrad et al.*, 1992] and small columns  $\sim 200$  grains in radius [e.g., *Hollenbeck and Jensen*, 1998].

Three types of gravity-stabilized phase invasion experiments were conducted: (1) equilibrium retention curve measurements, (2) transient outflow experiments starting from full initial saturation each using one of five different pressure steps, and (3) transient outflow experiments each using the same pressure step but starting from two different initial saturation structures containing entrapped gas. All experiments were conducted with two to five replicates. For all runs we simultaneously monitored the outflow volume from the cell, yielding macroscale response and the 2-D thickness-integrated saturation field yielding microscale behavior. Data acquisition and control were accomplished with a computer in order to ensure comparability of results. The total experimental period encompassed 7 weeks, of which the first 4 were used to settle the sand and refine our experimental procedure, while the experiments presented in this paper were performed during the final 3 weeks. In the following, we describe the components of the experimental system, methods, and experimental sequences in detail.

### 2.1. Cell Design

The cell assembly consisted of an inner glass cell containing sand held together within an outer glass frame (see Figure 1). The inner cell was constructed from two 2 cm thick glass plates held apart along opposite side edges by 1 mm thick spacing strips with 1.2 mm O ring gaskets along their inner edges. A porous plate made of sintered bronze (filtersize  $60 \mu\text{m}$ , Dansk Sintermetal A/S) with filter paper on top ran the full width of the cell and constituted the bottom boundary condition. The porous plate itself had a very low air entry pressure and thus

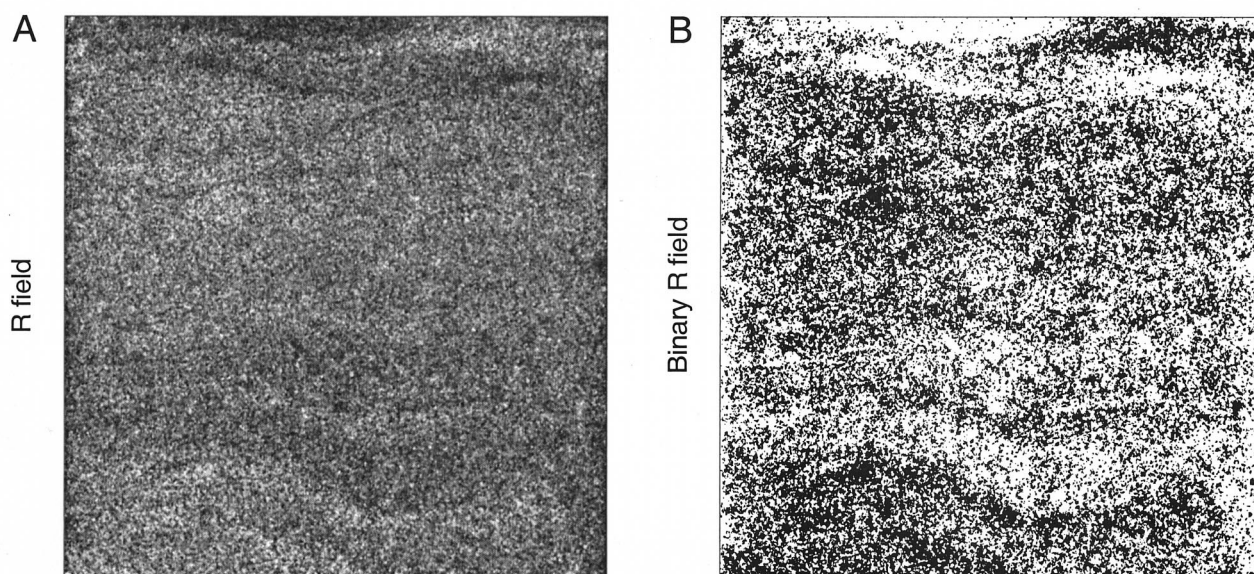


**Figure 2.**  $R$  field structure as determined using light transmission: (a) gray-scale image, where light indicates large  $R$  and dark indicates small; (b) binary  $R$  field, where white indicates  $R$  below the mean and black indicates  $R$  above the mean.

was used only to support the sand pack. Two layers of filter paper (an 8  $\mu\text{m}$  cellulose nitrate filter, Sartorius model 11301-293G, and a more sturdy qualitative cellulose filter paper, Whatman 1) provided an air entry pressure of over 120 cm. The bronze plate was installed flush within a piece of plastic; a small water reservoir underneath was connected to an outflow valve. The bottom boundary block was sealed to the cell with a 2 mm silicon gasket. Two needles penetrated the gasket and entered the cell, one at each side just above the filter paper. By applying a vacuum to the two needles and thereby pulling air through the cell the sand could be dried while still maintaining full saturation of the porous plate. The top boundary block distributed fluid across the cell width through a fine screen and was sealed to the cell with another silicon gasket. The inner glass cell was placed between two 2 cm thick glass plates, attached to an aluminum frame, and the frames were tightened together with screws to a uniform torque that held the entire cell together. The boundary blocks were tightened to the cell against the outer frames, and finally, the entire cell assembly was mounted horizontally in front of a constant light source. The volume of the inner cell was measured to be 13.0  $\text{cm}^3$ , with a visible zone of 9.43 cm wide by 9.79 cm high. The only portions of the cell that could not be monitored by light transmission were the  $\sim 2$  mm thick zones at the top and bottom of the cell where the silicon gaskets sealed the boundary blocks.

## 2.2. Sand Pack

The inner cell was packed with a subsample of a well-sorted rounded silica sand (grain distribution 0.18–1.65 mm, mean 0.4 mm, and standard deviation 0.1 mm) that was acid-washed to remove any organic residual. The subsample was simply poured into the cell through a funnel. Prior to the experiments the sand was settled by repeated cycles of saturation (see below) and drainage. We found that a large number of these cycles ( $>20$ ) were required to achieve a stable grain structure within the cell. During that period more sand had to be added

to the cell five times (total of  $\sim 2.6$  g added). The final amount of sand in the cell was 20.43 g, giving an average porosity in the cell of 0.41 and pore volume (PV) of 5.33 mL (assuming a grain density of  $\rho = 2.65 \text{ g cm}^{-3}$ ). During the final 3 weeks of experiments our procedures all worked to keep the sand pack stabilized with fluid flows occurring only from top to bottom of the cell. Further, sand settling during these experiments assessed through image analysis was undetectable over the majority of the cell. However, near the top, very slight compaction ( $<0.1$  mm or 1 CCD pixel) was noted.

Assuming that the difference in light adsorption between the fully dry and fully wet states is simply governed by refraction of a light ray normal to a series of flat grains/pores, we can make use of images at these two states to calculate an estimate of the number of pores at each location within the field [e.g., *Tidwell and Glass*, 1994]. Further, assuming that the local average pore radius  $R$  is inversely related to the number of pores (simple geometrical argument), we can estimate an  $R$  field for the sand pack as shown in Figure 2a. We see that the field is composed of a very slight set of gently undulating laminae where slightly smaller  $R$  (smaller grains) or larger  $R$  (larger grains) spanned the cell thickness. These laminae are typical in samples used to measure hydraulic properties and are caused by natural grading processes as granular materials are poured, vibrated, or otherwise mixed. We note that these laminae were difficult to see without application of the light transmission theory. For the purposes of later comparison to experimental results, we show a binarization of the  $R$  field at its mean in Figure 2b, where small  $R$  is shown in white and large  $R$  is shown in black.

The conductivity of the total system (sand and bottom boundary) was found to decrease slightly from  $4.1 \times 10^{-4}$  to  $3.7 \times 10^{-4} \text{ m s}^{-1}$  during the last 3 weeks of the experimental period. The hydraulic conductivity of the bottom boundary alone (porous plate and filter papers) decreased from  $7.2 \times 10^{-4}$  to  $1.0 \times 10^{-4} \text{ m s}^{-1}$  across the full 7 week period, possibly because of corrosion of the bronze plate or filtration of small



particles by the filter papers. Assuming a linear decrease in time for the conductivity of the bottom boundary, the change in total system conductivity over the critical 3 weeks can be fully explained, yielding a constant conductivity for the sand pack of  $4.2 \times 10^{-4} \text{ m s}^{-1}$ .

### 2.3. Saturation Procedure

For experiments that started from full saturation a standardized resaturation cycle was followed to ensure reproducible initial conditions. First, the cell was dried by applying a vacuum to the two needles, thereby pulling filtered (qualitative filter paper, Whatman 1) dry air through the cell. Second, the cell was flushed with  $\text{CO}_2$  for 30 min to displace the air. Third, the sand was saturated with freshly deaired, nanopure, deionized water, again, by applying a vacuum to the two needles and pulling water from the water reservoir rapidly down through the sand. Approximately 70 PV of water were then flushed through the sand and out both the needles and the porous plate to ensure complete dissolution of the  $\text{CO}_2$ . This procedure gave full saturation of the sand, as was verified by images taken during the saturation process.

### 2.4. Fluids, Boundary Conditions, and Outflow Measurement

Differential phase pressure for the outflow experiments was provided via a pressurized nitrogen gas container. The gas was humidified before the experiments to avoid evaporation of water in the cell during the experiment. First, the gas was bubbled through a porous stone and into a 10 L container half filled with water. Second, the humidified gas was led to another 10 L container, big enough to supply the cell with a constant pressure during the outflow experiments (the released gas volume from this second container was  $5.33 \text{ cm}^3$  at most). A solenoid valve was placed between the pressure container and the cell to control the start of the experiments. A water column was used to monitor the pressure both prior to each experiment, i.e., when the pressure in the container was adjusted to the desired step level, and during each experiment. During humidification the gas pressure always rose, and time was allowed for the pressure to stabilize before the experiments. However, minor pressure fluctuations occur very easily when using humidified gas; during the experiments, maximum fluctuations of  $\pm 3 \text{ mm}$  were recorded.

For outflow experiments, water dripped from a 5 cm long vertical tube directly into a beaker placed on a computer-monitored scale. Evaporation was restricted to a negligible rate with a specially designed beaker lid. Additionally, several precautions were taken to reduce the risk of algae growth in the cell during the course of the experiments. Deaired nanopure water was used for saturating the sand, and nitrogen was used to provide the necessary gas pressure. Only when drying the cell were water and oxygen present in the cell at the same time. The sand was always dry, and the cell was shielded from light between experiments. Finally, the laboratory was maintained at a temperature of  $21^\circ\text{C} \pm 0.5^\circ\text{C}$  to minimize fluid property variation.

### 2.5. Saturation Field Measurement

The cell was placed in front of a constant light source, and as the experiments proceeded, images were collected with a shuttered and electronically cooled charge-coupled device (CCD,  $1024 \times 1024$  pixels, 4096 gray levels) camera placed  $\sim 2 \text{ m}$  in front of the sample. Because the difference between the re-

fractive indices of the sand-gas and sand-water interfaces results in a significant reduction in light transmission as gas replaces water, the phase displacement process could be followed in exquisite detail [e.g., Glass *et al.*, 1989].

The acquired images contained  $943 \times 979$  pixels covering the entire sand-filled cell between the top and bottom boundary block gaskets with a resolution of  $0.1 \text{ mm} \times 0.1 \text{ mm}$  per pixel; thus an average grain of  $0.4 \text{ mm}$  was covered by  $\sim 16$  pixels. Images were collected as the experiments proceeded at a maximum temporal resolution of one image every seventh second, allowing for data storage operations. A high-frequency fluorescent light bank controlled with a feedback circuit was used as a near-constant diffuse light source. Still, the images were adjusted for small fluctuations in the light source intensity ( $\sim 1\%$  of the mean intensity). An optical density wedge, with five different steps covering the optical density range of the cell, was placed near the sand sample and incorporated into every image. The wedge thus provided a reference so that every image could be intensity adjusted to the same reference image. After this adjustment the images were analyzed for shifting, which can occur because of very small movements of the camera or cell during experiments (e.g., vibrations or thermal expansion). The shifts found were always  $< 1$  pixel (i.e.,  $0.1 \text{ mm}$ ) and corrected to a tolerance of 0.05 pixel. Further details on the intensity adjusting, shifting, and consequential error in the intensity fields are given by Detwiler *et al.* [1999]. Finally, the adjusted and shifted images were converted into quantitative saturation fields using a functional relationship based on light refraction theory [Tidwell and Glass, 1994]. Mass balance at the cell scale was used to calibrate the final saturation values. Comparison of transient outflow measured gravimetrically and through evaluation of saturation images yielded reasonable accuracy with differences  $< 1\%$  ( $< 0.05 \text{ mL}$ ) when changes were within the visible portions of the cell (i.e., not hidden by the boundary block gaskets).

### 2.6. Experimental Sequence for Retention Curve Experiments

Retention curve experiments were conducted five times during the last 3 weeks of the experimental period, three times before the outflow experiments and twice after the final outflow experiment. The experiments started from full initial saturation, and by connecting a water-filled semirigid tube to the outflow valve and manually lowering it in steps of 2.5 or 5 cm the bottom boundary suction was increased sequentially from 0 to 40 cm. At every step we awaited equilibrium and then weighed the amount of water drained from the cell. Throughout each experiment, images were acquired at 5 min intervals. Equilibrium was operationally defined when consecutive images no longer exhibited visible differences; between 30 and 110 min were required at each pressure step, yielding a total experimental time of  $\sim 12$  hours.

Different analyses of the measured data were used for determining the retention curve for the system. First, a traditional macroscale retention curve was found by plotting the mean saturation in the cell, calculated from the observed outflow, against the midcell suction. Second, the saturation fields recorded during the experiment were analyzed to yield subsample retention curves at a variety of scales and locations. Assuming equilibrium in the stabilized saturation fields, the vertical suction profile is hydrostatic, and corresponding values of saturation and suction are available throughout the cell. Two different approaches for determining the retention curves

from the saturation fields were used. Retention curves for different rectangular regions of interest (ROIs) were found by calculating the mean saturation of the ROI and plotting it against the suction of its middle for each pressure step. Also, horizontally averaged vertical profiles were constructed from each equilibrium saturation field, and when combined with the hydrostatic suction profile, profile retention curves from each equilibrium image were derived.

## 2.7. Experimental Sequence for Outflow at Different Pressure Steps

A total of 15 outflow experiments was performed on the cell, each starting from full initial saturation. First, an initial suction of 5 cm was applied to the bottom porous plate by opening the outflow valve. This drained the plumbing and boundary pores at the top of the cell and thus removed them from influencing experimental measurements. Second, after 10 min of equilibration, outflow was induced by applying pneumatic pressure in the nitrogen gas phase. We conducted experiments with five different pressure step applications, corresponding to a final suction at the bottom boundary of 17.5, 22.5, 27.5, 35, and 40 cm, respectively. These pressure steps all correspond to similar positions on the measured retention curve to those considered by *Hollenbeck and Jensen* [1998]. We conducted three replicates at each pressure step. The start of each one-step experiment was controlled by a computer that opened a solenoid valve to induce outflow and at the same time started scale readings and image acquisition. Every experiment lasted 57 min and yielded 48 images. In the early phase, when displacement was rapid, images were acquired every seventh second (the fastest acquisition possible), but as the outflow slowed, images were acquired every other minute.

## 2.8. Experimental Sequence for Outflow From Different Initial Saturation Structures

Four outflow experiments were performed to examine the effect of initial saturation and its structure on outflow. The experiments were performed with 5 cm of initial suction and a suction step level of 22.5 cm. The experiments followed the same procedure as in the previously described outflow experiments, but instead of full initial saturation, we changed the rewetting sequence to achieve an initial condition that contained entrapped air. Two different rewetting sequences that yielded significantly different entrapped structures were considered, each with two replicates. In the first the dry sand was not flushed with  $\text{CO}_2$  prior to the rewetting, as was practiced in the previous outflow experiments. Furthermore, rewetting was with nondeaired water and from below (through the porous plate) without flushing any water through the cell. In the second this same procedure was followed, but now the sand was not dried before rewetting. Instead, the cell was saturated from below after the conclusion of a retention curve experiment. Both these rewetting sequences are common practice, and thus we did not examine the effects of incomplete initial saturation systematically but rather in context of common laboratory procedures. As it happened, each sequence type gave nearly identical initial effective saturations ( $\sim 0.91$ ) but very different initial saturation structures within the cell.

## 3. Results

In the following we first present the results of the retention curve experiments and consider both invasion behavior and the

measurement of retention curves at a variety of scales. We then use this understanding in the subsequent presentation of the outflow experiments. There we first present the experiments from a saturated initial condition at various imposed pressure steps and, finally, experiments from varying initial saturations at a single imposed pressure step.

### 3.1. Retention Curve Experiments

Example equilibrium saturation fields for suction steps of 15, 17.5, 20, 22.5, 25, and 27.5 cm are presented in Figure 3 and show the advance of a near-horizontal, gravity stabilized drainage front downward through the cell. At all suctions the furthest penetration of the air phase or front exhibits a visually complicated pattern containing a wide range of length scales. Behind the front, visual phase structure complication generally decreases because of a corresponding decrease in the longer length scales and a uniform increase in the air phase saturation. This structure can be described in the context of gradient percolation [*Wilkinson*, 1984] where capillary fingers at the front move downward and create a wide range of length scales, the extent of which are limited by competition with gravity forces. Behind the invasion front the wetting phase does not become trapped by the invading gas and can continue to drain from pockets through connected pores or possibly via film flow. The influence of heterogeneities is apparent both at the front where they influence the growth of capillary fingers and behind the front where smaller pores hold onto water at higher suctions than the larger pores.

The saturation field at the 27.5 cm suction step is anomalously different in character from all lower suction states. Careful study of the transient images shows that at each change in the boundary suction the invasion front moves rapidly downward into the cell followed by subsequent “back filling” by air. Some additional advance of the front also occurs during the back-filling stage with multiple pore Haines jumps clearly evident and spaced widely in time. For all suction steps below 27.5 cm the complication of the saturation structure thus first increases and then decreases as the system moves toward equilibrium. However, when the suction is increased to 27.5 cm, gas fingers rapidly downward to the porous plate near the left side of the cell, moves horizontally at the boundary across the full cell width, grows upward, and then all further outflow essentially stops. Accordingly, the gas structure changes insignificantly at the higher suction steps (35 and 40 cm, not shown here). Obviously, flow through the desaturated region at the bottom of the cell has been drastically reduced, and thus the further drainage of the large fully saturated regions left above is curtailed at the timescale of the experiment. This near isolation of the experimental system from the exit boundary effectively freezes the complicated invasion structure without allowing the subsequent back filling seen at lower suctions.

To explain the invasion front movement within the cell, we first consider the horizontally averaged profile retention curves for the saturation fields below 27.5 cm (see Figure 4). We see a systematic trend with the curves rising as the position of the gas invasion front penetrates farther into the cell. Between the 15 and 25 cm profiles the curve has risen  $\sim 6$  cm, indicating a decrease in the mean radius of the pores,  $\langle R \rangle$ , at the invasion front by a factor of  $\sim 0.79$  at this position. This decrease in  $\langle R \rangle$  appears smooth and linear from the top of the cell until the front extends to  $\sim 3\text{--}4$  cm from the bottom. At this point,  $\langle R \rangle$  must decrease, and the invasion front moves downward the full distance to the bottom boundary as a capillary finger. If we now



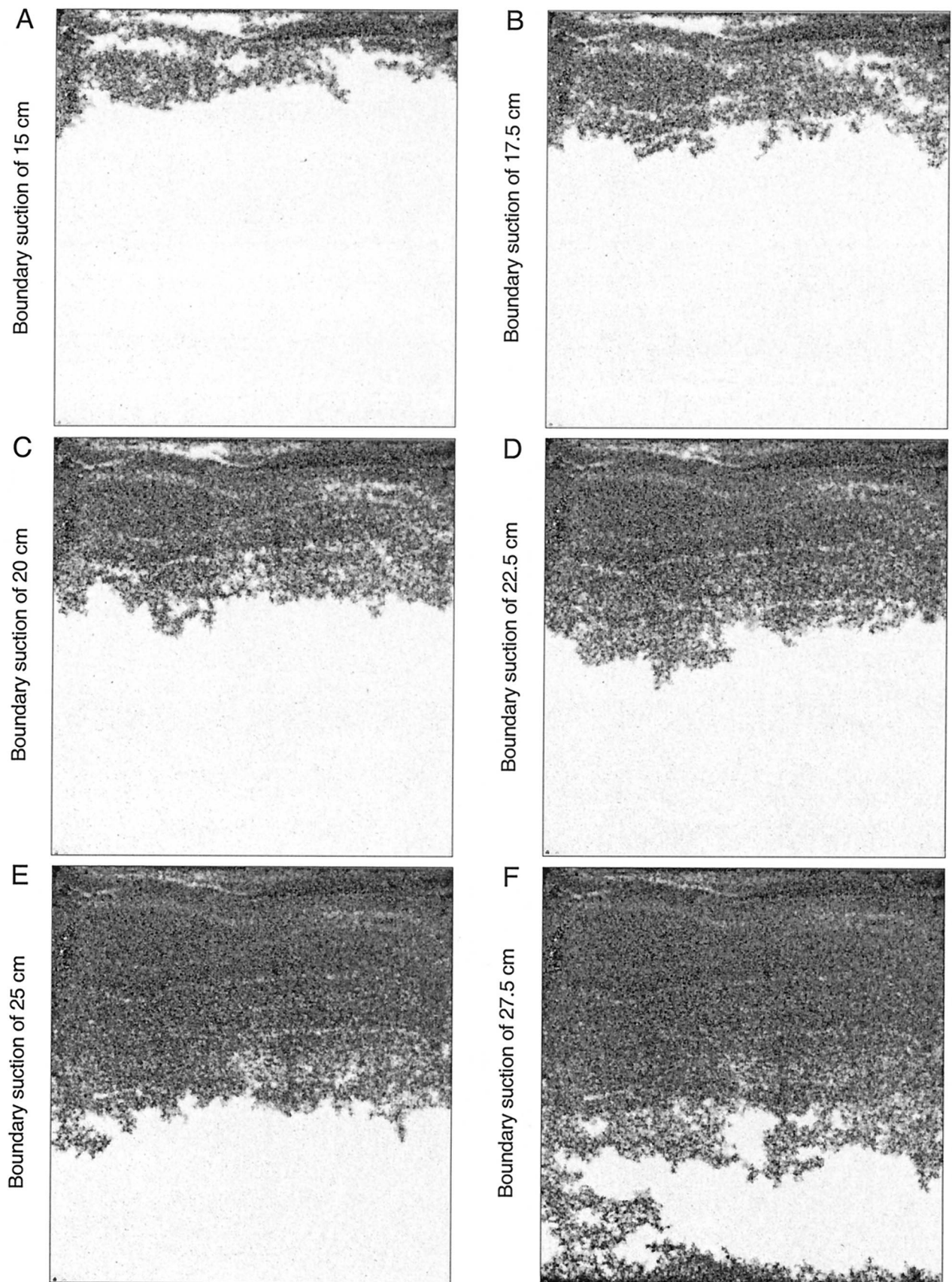


**Figure 3.** Example of final stabilized saturation fields from a retention curve experiment at intermediate boundary suctions of 15, 17.5, 20, 22.5, 25, and 27.5 cm. Light indicates saturated areas, and dark indicates less saturated areas.

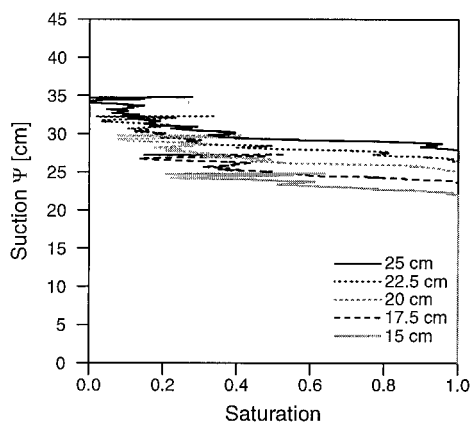


**Figure 4.** Example of profile retention curves determined from the final stabilized saturation fields at intermediate boundary suctions of 15, 17.5, 20, 22.5, and 25 cm (corresponding to the images presented in Figure 3).

consider Figure 2a and the binarized field in Figure 2b, we clearly see the control placed on the invasion process by the  $R$  field. Black regions corresponding to large pore regions map well the gas phase near the invasion front in each saturation image. We also see the zone where the gas finger breaks down to the bottom boundary to be clearly of larger  $R$  directly below a strongly connected region of small  $R$ . Thus we find a capillary barrier configuration with a direct failure pathway to the bottom boundary when it breaches. Finally, sand along the bottom boundary must form a zone of connected larger pores. Its presence in combination with the larger  $R$  in the sand immediately above (see Figure 2a) forms a strong width spanning heterogeneity beyond that of a simple edge or wall effect.

Macroscale retention curves determined from the measured outflow are presented in Figure 5. As a consequence of the microscale processes acting within the experiment described above, the curves exhibit no discernible air entry pressure and a rather high residual water saturation ( $\sim 0.41$ ) beginning at only 27.5 cm. The lack of a defined entry pressure is due to the size of the sample relative to the changes in saturation across the height of the cell. The high residual value is associated with the combination of internal heterogeneity, capillary fingering, and width spanning bottom boundary heterogeneity, which effectively isolates the cell from further drainage.

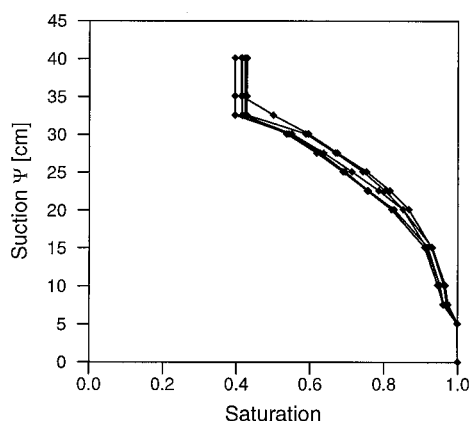


**Figure 5.** Macroscale retention curves (five replicates) determined from measured outflow and midcell level suction.

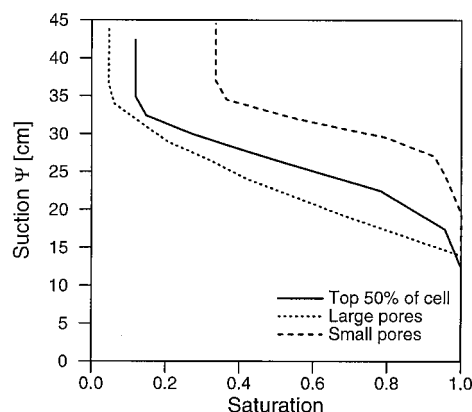


**Figure 6.** ROI (region of interest) retention curves determined from the stabilized saturation fields.

If we consider ROI-based curves determined within the top 50% of the cell, we find more reasonable residuals and much sharper transitions (see Figure 6, note residuals are dependent on system isolation). Within this large region we can also consider smaller regions containing mainly small or large pores. These curves are slightly sharper and show differences in their height (air entry pressure) as well as in their residuals. Averaging such regions yields the average behavior seen in the large top ROI curve. The differences between these measurements is not simply a function of scale in interaction with heterogeneity but also the accessibility of the various pores to the nonwetting fluid. Note that if we considered an ROI-based measurement of retention in the region at the bottom of the cell, we would obtain a very sharp curve with an air entry value of  $\sim 27.5$  cm. However, this entry value is controlled by the zone of small pores several centimeters above. All of these results point to the control of system response and thus to property measurements by heterogeneity, connectivity, and ac-

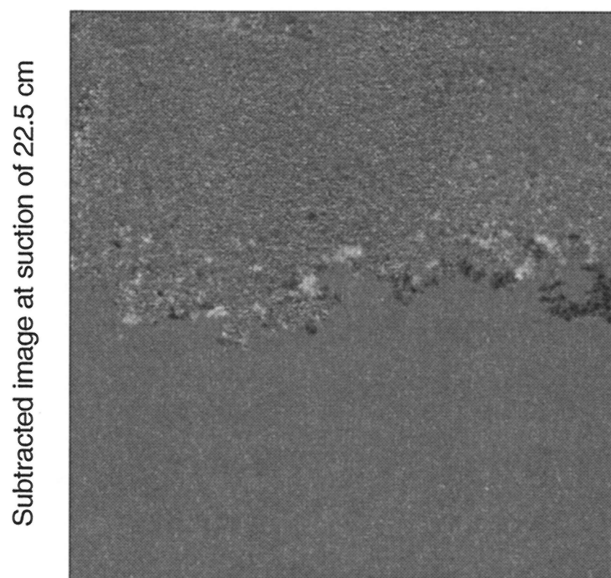


**Figure 7.** Subtraction of two stabilized saturation fields from two different retention curve experiments (intermediate boundary suction of 22.5 cm). Light and dark indicate differences between the two saturation fields; gray indicates no differences.



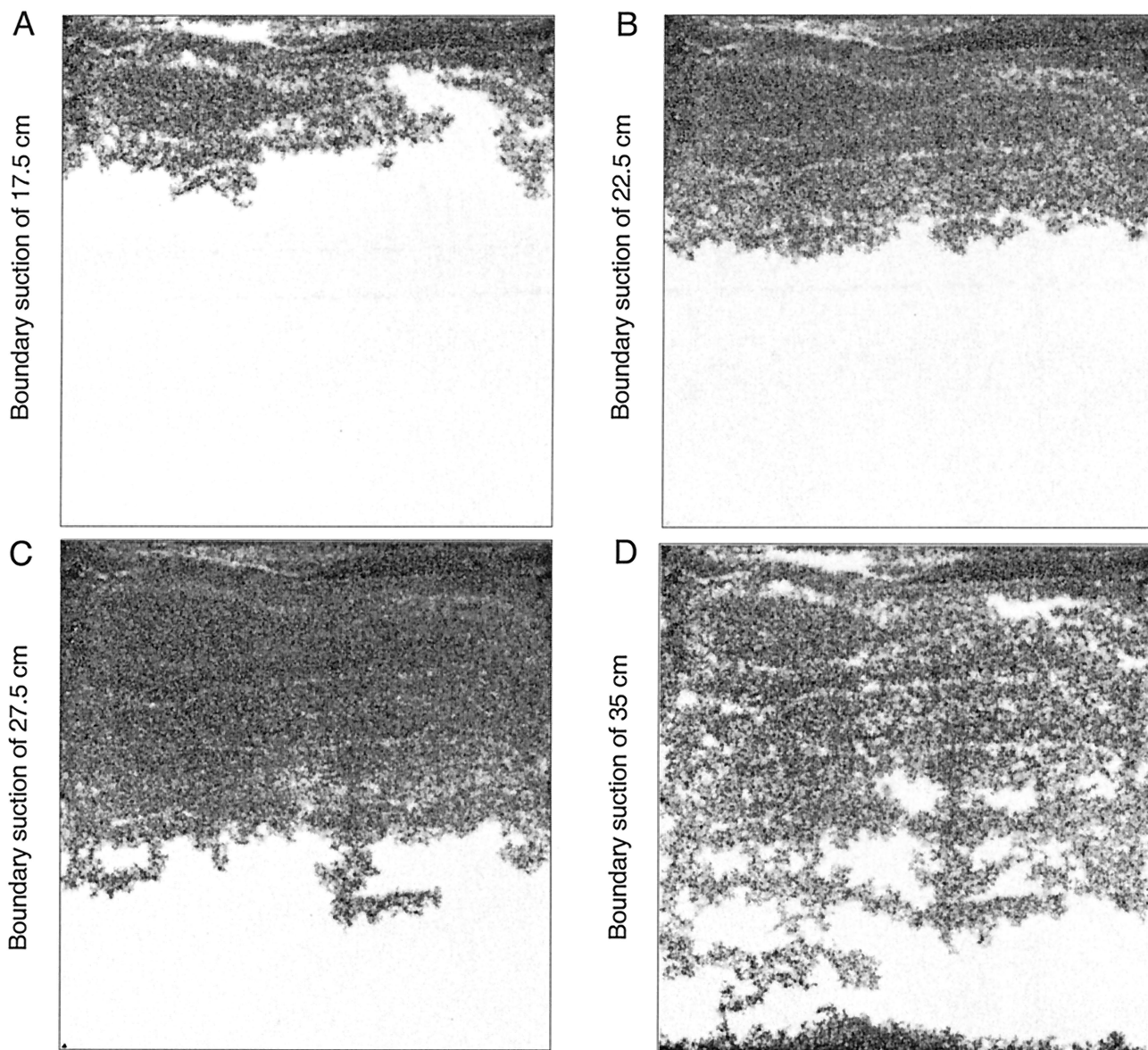


**Figure 8.** Example of final saturation fields from one-step experiments with boundary suctions of 17.5, 22.5, 27.5, and 35 cm.

cessibility within the domain where capillary, gravity, and viscous forces interact. In particular, the behavior at the 27.5 cm suction step foreshadows boundary condition sensitivity in the one-step outflow experiments to be presented below.

Saturation fields from replicate retention curve experiments are effectively identical; however, each invasion structure at each equilibrium state as well as the exact evolution path is slightly different (see Figure 7). These differences are mainly seen at the front and are due to the different extents of various capillary fingers, thus yielding a clumped or spatially correlated discrepancy between experiments. Behind the front, differences decrease, become more evenly distributed, and are at the scale of individual pores. Comparison of the different retention curve experiments also highlights the critical heterogeneity that controls system behavior at the 27.5 cm suction step. Of the five retention curves measured, four of them show this same behavior; however, one required the 30 cm step before the gas finger extended to the bottom boundary and isolated

the system from subsequent drainage (see Figure 5). Once this occurred, the final effective saturation structure was identical to the other experiments within the typical variability discussed above.

### 3.2. Outflow Experiments at Different Pressure Steps

Example final saturation fields from the experiments performed with pressure steps of 17.5, 22.5, 27.5, and 35 cm are presented in Figure 8. The final saturation field for the experiment at 40 cm (not presented here) was effectively identical to that at 35 cm. Measured cumulative outflow curves for the five different sets of outflow experiments are presented in Figure 9, with the results for small pressure steps (17.5, 22.5, and 27.5 cm) grouped in Figure 9a and those for large pressure steps (35 and 40 cm) grouped in Figure 9b. The total amount of water drained in the different experiments first increases with boundary suction, yielding mean values of 0.19 PV at 17.5 cm, 0.33



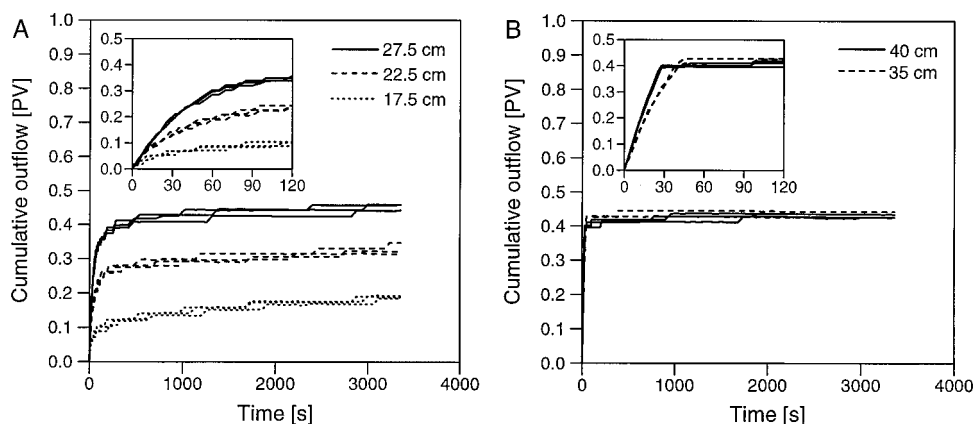


**Figure 9.** Measured cumulative outflow (pore volume) for one-step experiments at (a) small pressure steps (17.5, 22.5, and 27.5 cm) and (b) large pressure steps (35 and 40 cm). The insets show the early time behavior.

PV at 22.5 cm, and 0.45 PV at 27.5 cm and then decreases to 0.43 PV for both 35 and 40 cm (see Table 1).

We see two distinct types of response exhibited in the experiments, one for small pressure steps (27.5 cm and below) and another for large (35 cm and higher). Both of these behaviors are anticipated by the results and discussion of the retention curve experiments above and are further illustrated with intermediate images at 14 and 38 s from the experiments using 27.5 and 35 cm steps in Figure 10. At small pressure steps, water drains rapidly in the beginning and then slows as equilibrium is approached (note that the jagged nature of the outflow curves (Figure 9a) at late time is artificial and corresponds to dripping onto the scale). This outflow behavior corresponds to the rapid movement of air into the cell at the beginning of pressurization (Figure 10a), after which pockets of water are slowly back-filled by air (Figure 10b). At large pressure steps, water drains rapidly but then abruptly stops after  $\sim 1$  min. We see from the saturation fields that rapid air fingering through the sand (Figures 10c and 10d) reaches the bottom boundary, moves horizontally along the porous plate, and creates a capillary barrier that blocks further drainage, just as is seen in the retention experiments. Thus at small pressure steps, drainage is restricted to the upper part of the cell, and back filling can occur to completion, but at high pressure steps, pronounced air fingering to the bottom boundary and subse-

quent isolation of the system freezes a highly complicated air invasion structure in the final state and yields a lower effective saturation. For both cases the gas invasion structure at the front or throughout if back filling cannot occur is highly correlated to the structure of large  $R$  in Figure 2b.

The final saturation fields from outflow experiments can be compared with those from corresponding steps in the retention curve experiment. At 17.5 and 22.5 cm the final saturation distributions for the one-step outflows are very similar to those seen in the retention experiments (compare Figures 3b and 3d with Figures 8a and 8b). However, the air front has penetrated slightly farther in the retention curve experiment. At 27.5 cm, gas breaks through to the porous plate in the retention curve experiments, while this has yet to occur in the outflow experiments (compare Figures 3f with 8c). These differences cannot be accounted for by either variation of fluid properties or boundary conditions. Rather, the differences are explained by the discrepancy in the timescales of the two types of experiments. Differences increase as we consider larger differential pressures, and evaluation of the images at the end of the 57 min outflow experiments showed that water was still draining at a very low rate from the 27.5 cm experiment. At higher-pressure steps the differences between outflow and retention curve experiments change character and thus become more marked (compare Figures 3f with 8d). While in the retention

**Table 1.** Number of Pore Volumes Drained in the Retention and One-Step Experiments When Increasing the Boundary Suction from 5 to 17.5, 22.5, 27.5, 35, and 40 cm, respectively<sup>a</sup>

	17.5 cm	22.5 cm	27.5 cm	35 cm	40 cm
Retention curve	0.19	0.33	0.50	0.59	0.59
	0.20	0.33	0.57	0.57	0.57
	0.21	0.36	0.59	0.59	0.59
	0.25	0.38	0.58	0.58	0.58
	0.24	0.37	0.60	0.60	0.60
One-step full saturation (A)	0.18	0.35	0.44	0.43	0.43
	0.19	0.31	0.46	0.44	0.43
	0.19	0.32	0.46	0.43	0.43
One-step varying saturation (B)	—	0.26	—	—	—
	—	0.27	—	—	—
One-step varying saturation (C)	—	0.35	—	—	—
	—	0.34	—	—	—

<sup>a</sup>The retention experiments were reproduced 5 times; one-step experiments with full initial saturation (A) were reproduced 3 times; one-step experiments from varying initial saturation structure were reproduced twice using two different saturation procedures: (B) sand rewetted from below without previous CO<sub>2</sub> flushing and (C) sand rewetted from below without previous drying and CO<sub>2</sub> flushing.

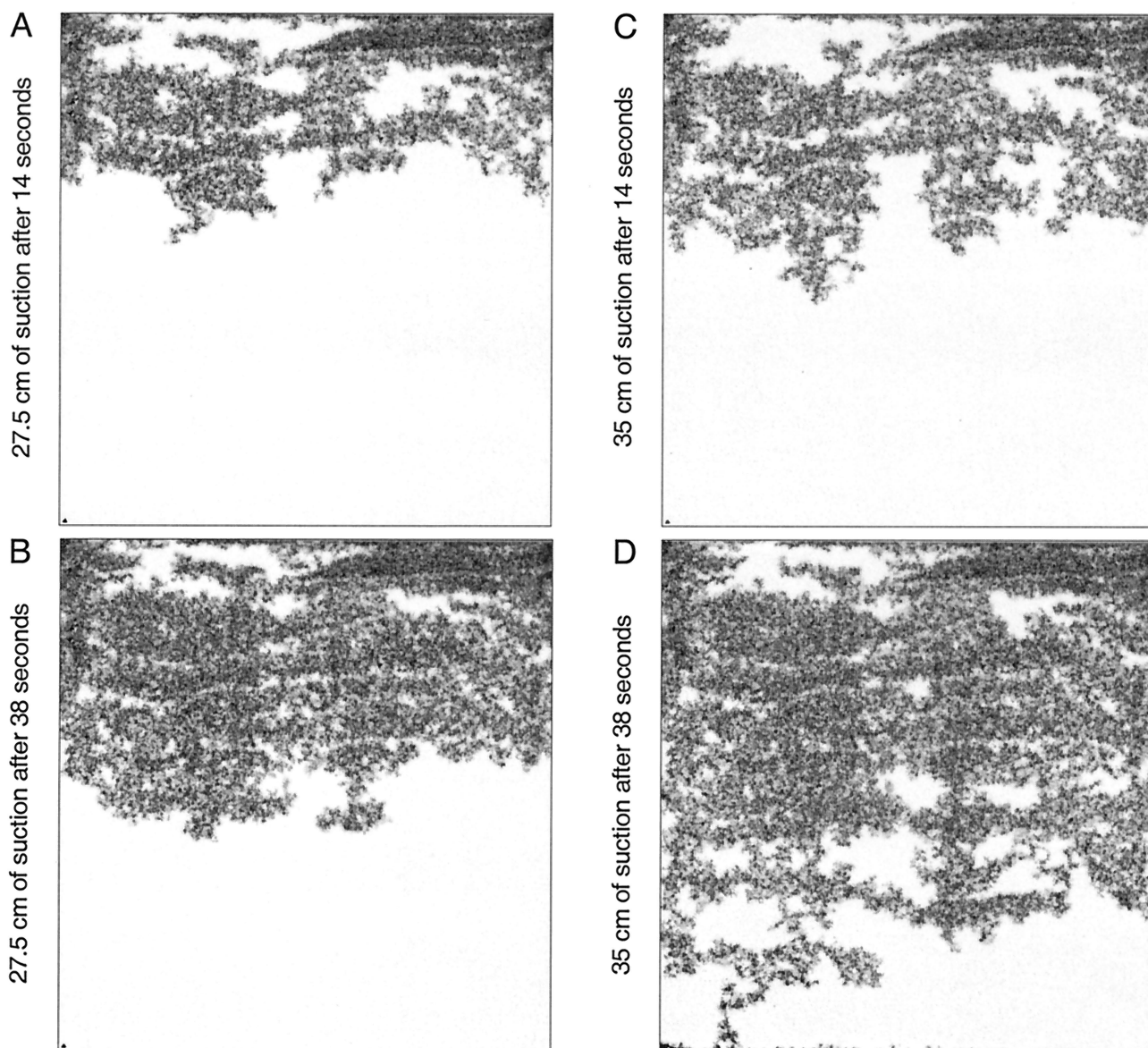


**Figure 10.** Example of intermediate saturation fields from one-step experiments with boundary suctions of 27.5 and 35 cm at 14 and 38 s (the final stabilized saturation fields are presented in Figures 8c and 8d, respectively).

experiment, back filling can occur up until the 27.5 cm step; it cannot occur in the outflow experiment where air fingering rapidly spans and then isolates the cell. This gives rise to a decrease in the final effective saturation of the system from 0.57 for the outflow experiments to 0.41 for the retention experiments at 35 cm and above. Thus, in context of a system width spanning heterogeneity the displacement speed as imposed by the boundary pressure step has a significant control on the microscale structural evolution and thus on outflow response and final effective saturation.

The replicate experiments show only minor differences in outflow response, and final saturation images are identical on a macroscopic level. However, at the microscale, evolution paths are slightly different, and no two final states are exactly the same (see Figure 11). These differences are similar in degree and behavior to those seen in the retention experiments described above. As another check on repeatability, we con-

ducted two additional one-step experiments where the pressure step was applied as a suction in the water by connecting a tube to the outflow valve that ran directly into a water-filled container on the scale located at the appropriate position below the cell. These experiments showed identical response (including slight randomness) to those using pneumatic pressure except, of course, the scale response was smoother because the water flowed directly into the container instead of dripping from the outflow valve.

### 3.3. Outflow Experiments From Varying Initial Saturation Structures

Examples of both the initial and the final saturation fields from each of the two sets of experiments performed from incomplete initial saturation are presented in Figure 12. Figure 12a shows the initial saturation field achieved by the first set where the dry sand was rewetted from below without previous



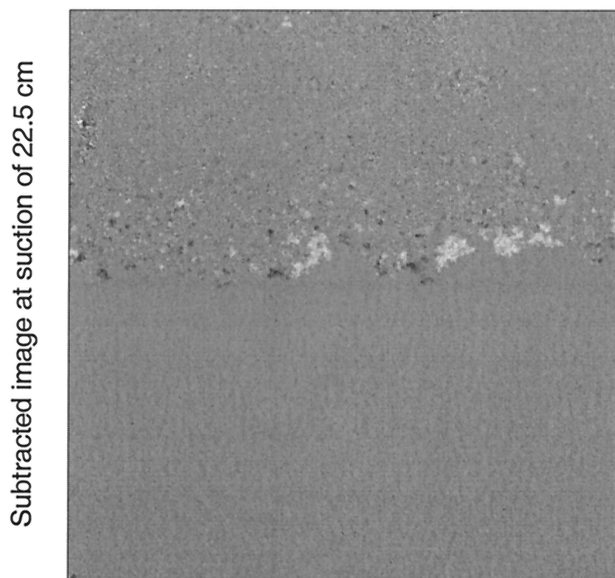


**Figure 11.** Subtraction of two stabilized saturation fields from two different retention curve experiments with boundary suction of 22.5 cm. Light and dark indicate differences between the two saturation fields; gray indicates no differences.

CO<sub>2</sub> flushing. In the middle of the cell the mean initial saturation is high ( $\sim 0.97$ ), with only a few residual air pockets. The regions near the top and bottom boundaries, however, are at lower saturation, especially above the porous plate (mean saturation of  $\sim 0.74$  in the top of the field and  $\sim 0.35$  in the bottom). Images acquired over the course of the rewetting sequence show that the water enters the cell through a few points at the bottom boundary and then expands laterally above the coarse heterogeneity, entrapping a large gas-filled region above the porous plate. The final saturation field at the end of the outflow experiment is presented in Figure 12b, showing the air invasion front to be very similar to that for the experiment from full initial saturation (Figure 8b).

An initial and final saturation field from the second set of experiments are presented in Figures 12c and 12d, respectively. This set of experiments was performed after a retention curve experiment, and since the sand was not dried prior to rewetting, the air-water structure before rewetting was as shown in Figure 3f. During the rewetting sequence, air became entrapped everywhere it was initially present, especially above the porous plate (compare Figures 3f and 12c). The middle of the cell had an initial saturation with a mean of  $\sim 0.93$ , and the top and the bottom had values of  $\sim 0.84$  and  $\sim 0.67$ , respectively. The final saturation field (Figure 12d) shows that the drainage front has moved farther down into the cell in comparison to the final saturation field obtained after full initial saturation (Figure 8b).

Outflow curves are compared with the corresponding one-step experiments from full initial saturation in Figure 13. The outflow curves observed in the experiments starting from incomplete saturation are generally more gradual than those observed in the experiments starting from full initial saturation. As before, replicates for each set of experiments show only minor differences within sets, but between the three sets, significant variation in cumulative outflow is apparent (see Table 1). Rewetting the dry sand from below without CO<sub>2</sub> flushing resulted in the least outflow, with a cumulative mean

of 0.27 PV, compared with the experiments performed from full initial saturation where the mean is 0.33 PV. In the experiments where the sand was not dried prior to the rewetting, the cumulative outflow is highest with a mean of 0.35 PV.

These results highlight the control imposed by the initial saturation structure on the outflow experiment. For both sets of experiments the mean initial saturation for the sample as a whole was nearly identical and high (0.91). However, the significantly more gradual outflow is controlled by the width-spanning low-saturation zone found in both experiments above the porous plate, which restricts the rate at which water can drain from the cell. Beyond this similarity the structures of the initial saturation fields were very different, and these differences additionally controlled outflow response. Rewetting the dry sand from below resulted in unsaturated areas at both boundaries with almost no gas entrapment between. Thus we find a nearly identical gas invasion structure as in the initially saturated case but a smaller cumulative outflow due to the lower saturation at the top of the cell. Skipping the initial drying step resulted in air entrapment throughout the middle of the cell as well. Because the initial gas-phase structure occupies clusters of pores, which when connected to the invading front yield a much greater accessibility for the invading phase, the front penetrates farther than in the initially saturated system and yields a larger total outflow.

Finally, we note that with respect to variation across replicates we find identical levels and behavior of differences, as previously described above for the retention and other outflow experiments. This similarity also extends to each replicate saturation sequence where identical initial effective saturations and structures occurred but small microscale differences, comparable to those seen in Figures 7 and 11, remain.

#### 4. Discussion

The heterogeneity within our sand pack is very slight and probably less than expected in samples where hydraulic properties are often measured. Yet its influence is marked. The primarily horizontal structure of these heterogeneities imparts a capillary barrier behavior to the pack with gas entry values interrogated by the drainage front that range  $\sim 12\%$  of the average value ( $\sim 26 \pm 3$  cm, see Figure 3). The presence of the bottom boundary and a zone of large  $R$  directly above also created a width-spanning heterogeneity with a gas entry value on the low end of this distribution. The influence of this bottom heterogeneity was amplified through combination with a well-connected zone of high gas entry value  $\sim 3$  cm above that formed a strong capillary barrier. While one could regard this behavior as edge effect, we believe it speaks more generally to the concept of width-spanning heterogeneity, as often present in experiment and nature alike.

We took extreme care to achieve high experimental accuracy and precision. This allowed excellent repeatability; however, for all replicates, minor differences were always found. These could have been the result of small fluid property differences (temperature), slight fluctuations in the gas pressure, and in the case of the retention curve experiments, slight differences in the equilibrium time at each step. However, it is also likely that the differences are due to inherent randomness within the drainage field as a myriad of pores are made accessible to the invasion front. In general, this randomness may average out as the system enlarges. However, when considering heterogeneities, randomness can also be accentuated if a critical hetero-

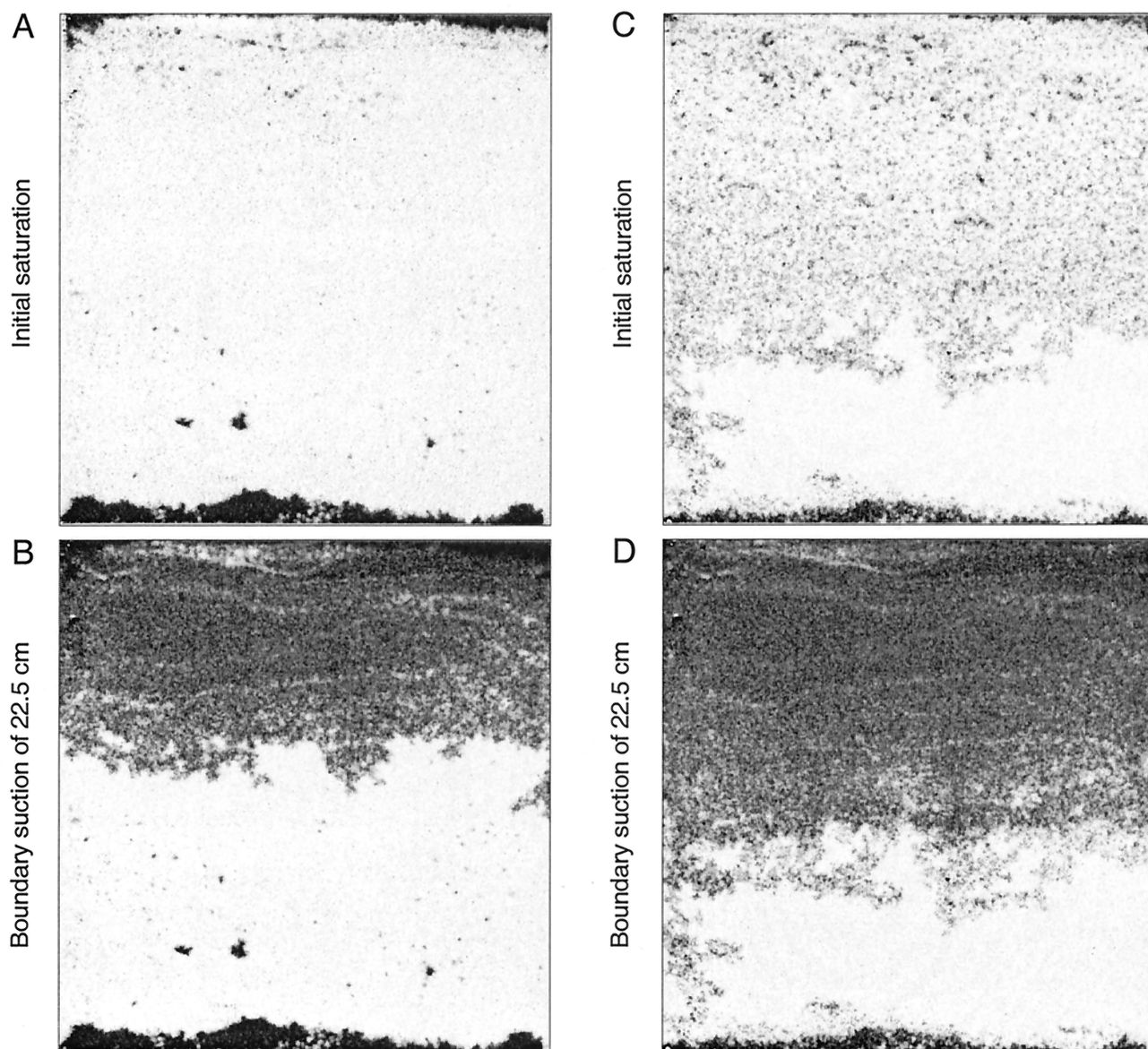


**Figure 12.** Example of initial and final saturation fields for one-step experiments with boundary suction of 22.5 cm from varying initial saturation structure: (a) and (b) sand rewetted from below without previous  $\text{CO}_2$  flushing and (c) and (d) sand rewetted from below without previous drying and  $\text{CO}_2$  flushing.

geneity is restricting advance of the drainage front, which, once breached, opens a large zone of media for entry by a now overpressured fluid. This constitutes a macroscale Haines jump controlled by heterogeneity in the pore network. Small fluctuations in the time to achieve the jump pressure or its being near the pressure supplied at a boundary can lead to significant differences. This is exemplified in comparison of the 27.5 cm final saturation fields for the retention and outflow experiments. Additionally, because of the control on local velocities imposed by such jumps, viscous forces can influence the structure during the jump differently than in the rest of the domain.

Considering viscous influences at the macroscale, when we increase the system-scale macro gradients imposed through changes in the boundary conditions, we obtain an interaction that exhibits significant qualitative and thus process-originated trends. This is controlled by the interaction of two microscale processes, the initial or rapid advance of the invasion front and

the slower back filling of pores behind. Because of the very different viscosities of the gas and liquid, the complication of the phase structure within the network influences each phase differently. At the invasion front, liquid can easily move toward the exit through saturated media, and gas can easily advance through the tortuous path behind because of its low viscosity. The liquid behind the invasion front, however, must now move through a tortuous path, the tortuosity of this path growing significantly with decrease in effective local saturation. Because of the viscosity of the liquid, resistance within this zone slows the back-filling process relative to frontal advance. Thus the timescales for frontal advance and subsequent back filling are very different. Additionally, when clusters of pores filled with liquid are separated from the bulk liquid, the timescale for back filling once again increases as drainage must now occur through films along the surfaces of grains. Superimposing an initial saturation field structure primarily influences the ad-



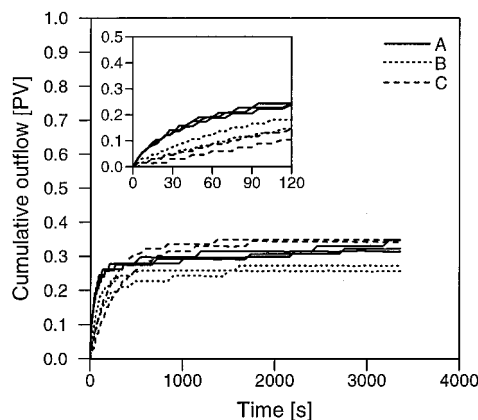


**Figure 13.** Measured cumulative outflow (pore volume) for one-step experiments with boundary suction of 22.5 cm using different saturation procedures: (a) sand rewetted from top after  $\text{CO}_2$  flushing (100% saturation), (b) sand rewetted from below without previous  $\text{CO}_2$  flushing (91% saturation), and (c) sand rewetted from below without previous drying and  $\text{CO}_2$  flushing (91% saturation). The inset shows early time behavior.

vance of the invasion front. Increased resistance to flow of the liquid ahead of the invading front decreases its speed and thus the outflow flux at early times. This effect is most dramatic when the trapped gas structure creates an in-series effect such as we had at the width-spanning heterogeneity at the bottom boundary. Additionally, accessibility at the invasion front to the gas is greatly enhanced by initial gas entrapment, allowing the front to advance farther into the system with increased outflow.

Because of the control placed by subsample-scale heterogeneity, initial saturation structure, and boundary condition on experimental response, variability or perceived randomness in systems where these vary a bit from one experiment to another is easily conceived. As mentioned in section 1, *Hollenbeck and Jensen* [1998] performed multiple outflow experiments on a cylindrical suction cell (diameter 6.35 cm and height 5.7 cm) with a sand similar to that used in this study. Their one-step outflow results had two key features: (1) at small pressure steps the outflow was poorly reproducible, and (2) at large pressure steps, outflow responses were identical even for different pressure steps. The level of randomness seen by *Hollenbeck and Jensen* [1998] at small pressure steps was not found here in replicate experiments for any pressure step or initial saturation structure. However, the saturation procedure used in this earlier work resulted in incomplete initial saturation (mean of 0.886 PV with a standard deviation of 0.01 PV) with different initial saturation structures expected for every experiment. On the basis of our results it is likely that differences in the saturation structure within the sample yields the perceived randomness they observed. The identical outflow responses seen for large pressure steps in this earlier work were also found in the experiments presented here. Therefore it is also likely that rapid air fingering with the subsequent isolation of the porous plate took place in their cylindrical cell as well.

We note that *Hopmans et al.* [1992] also visualized water distribution during one-step outflow experiments using X-ray computed tomography (CT) in cylindrical samples (diameter of 7.6 cm and height of 6.0 cm). They also found nonuniform drainage and air blockage at the porous plate when the system was initially saturated and correctly concluded that property

inversion is problematic in such situations. As discussed above, both retention and outflow experiments demonstrate the drainage process to be composed of rapid invasion composed of fingers with subsequent slower back filling by air. We see internal heterogeneity, especially when width spanning, as well as the initial saturation structure to combine with the phase invasion process imposed by the boundary condition to both control rapid invasion and limit the slower back-filling process under conditions of higher flow (larger step). While inversion of experimental data would yield reasonably precise property model parameters for a given outflow experiment (e.g., pressure step and initial saturation structure), these parameters will be different for each step and for each initial saturation structure. On an effective level this forces both relative permeability and retention curves as well as effective saturation to be path-dependent functions of both boundary and initial conditions. Additionally, initial conditions cannot be specified as a simple effective average because these macroscale properties will be sensitive to its initial structure. Others have suggested that additional physics must be considered for a more comprehensive description of unsaturated flow and must include the influence of, for example, interfacial areas and the momentum of interfaces [e.g., *Gray and Hassanizadeh*, 1998]. However, these approaches are rooted in the theory of volume averaging. Our experiments demonstrate that connectivity and accessibility, in conjunction with microscale processes, will provide a severe challenge to these approaches as well. Internal structure that controls macrosystem response is a path-dependent function of initial and boundary conditions that must be properly reflected in any volume-averaged approach.

Finally, we consider possible constraints on our results due to the nature of our experimental system. Our system was designed specifically to allow quantitative visualization of microscale processes with techniques that forced a thin but extensive pore network. The network is similar to a cross-section through a 10 cm tall by 10 cm diameter sand column. However, even though the pore network is 3-D, it lacks full connection out of its plane such as would occur in a sand column. Additionally, because the sand pack is only  $\sim 2$ –4 grains thick, the walls of the cell force a significant organization on the grains and thus pore network. Since organization from a wall extends many grains into a porous pack, our system is strongly influenced by close proximity of the two walls. If we consider a sand column, wall effect creates a large discrepancy between the edges of the sample and the interior. In our cell we contend this discrepancy is minor, and thus, while the wall significantly modifies our pore structure, we are actually left with a minimal wall effect. The fact that we did not find gas to move preferentially down along the side edges of the cell supports this contention. Along the bottom boundary, however, we did have an obvious edge effect, but the behavior is also correlated with slightly coarser material at the bottom (see Figure 2), as occurred when our barely graded subsample (coarser on top) was simply poured (inverted) into the cell. Because the experiments of *Hollenbeck and Jensen* [1998] with the same sand found similar macroscopic behavior in a sand column, we believe that our current results are indeed qualitatively representative of the microscale processes that occurred in their cylindrical cell as well. As a final proviso, we note that we have only performed experiments on a single porous medium representing relatively well graded medium-coarse sand. However, we suspect that the microscale processes observed in our system will be of general occurrence in column experiments and arbi-

trary porous media. Thus our results suggest general limitations to both the experimental estimation of hydraulic properties from traditional laboratory procedures and the theoretical conceptualization embodied in traditional continuum-based models for unsaturated flow.

## 5. Conclusion

We were interested in the causes of discrepancies in sample-scale effective behavior between repeat experiments, between different types of experiments, boundary or initial conditions, and, most importantly, between experimental behavior and that predicted or implied by standard continuum conceptual models for unsaturated flow in porous media. Our visualization experiments have revealed microscale phase invasion processes that control macroscale experimental response in experiments commonly employed to measure unsaturated flow properties. These experiments illustrate the interaction between slight subsample heterogeneity, imposed boundary pressures or fluxes, and initial saturation and its structure to control the qualitative and quantitative behavior of the microscale-phase invasion process. Randomness, while present in our experiments, is small. However, its influence can be accentuated by heterogeneity in combination with critical values of boundary pressures. Experiments with different boundary conditions, sequences, and timescales yield strong qualitative differences in experimental response. Likewise, different internal initial saturation structures with the same sample-scale effective value also yield significant differences. These qualitative differences signify a varying influence of different microscale processes and thus a deviation from unique standard continuum-scale behavior and accompanying hydraulic properties.

**Acknowledgments.** We thank Lee Orear, Will Peplinski, and Anthony Chavez for their help in cell construction and setup of experimental apparatus. RJG acknowledges funding from the U.S. Department of Energy's Basic Energy Sciences Geoscience Research Program (contract DE-AC04-94AL850000). APM acknowledges funding from the Danish Strategic Environmental Research Program. Experiments were conducted at the Flow Visualization and Processes Laboratory at Sandia National Laboratories. Results contained in this paper were originally presented by Mortensen *et al.* [1998] at the 1998 Fall AGU meeting.

## References

- Buckingham, E., *Studies on the Movement of Soil Moisture*, Govt. Print. Off., Washington, D.C., 1907.
- Conrad, S. H., W. R. Mason, W. J. Peplinski, and J. L. Wilson, Visualization of residual organic liquid trapped in aquifers, *Water Resour. Res.*, 28(2), 467–478, 1992.
- Corey, A. T., *Mechanisms of Immiscible Fluids in Porous Media*, Water Resour. Publ., Highlands Ranch, Colo., 1985.
- Detwiler, R. L., S. E. Pringle, and R. J. Glass, Measurement of fracture aperture fields using transmitted light: An evaluation of measurement errors and their influence on simulations of flow and transport through a single fracture, *Water Resour. Res.*, 35(9), 2605–2617, 1999.
- Glass, R. J., T. S. Steenhuis, and J.-Y. Parlange, Mechanism for finger persistence in homogeneous, unsaturated, porous media: Theory and verification, *Soil Sci.*, 148, 60–70, 1989.
- Gray, W. G., and S. M. Hassanizadeh, Macroscale continuum mechanics for multiphase porous-media flow including phases, interfaces, common lines and common points, *Adv. Water Resour.*, 21, 261–281, 1998.
- Hollenbeck, K. J., and K. H. Jensen, Experimental evidence of randomness and nonuniqueness in unsaturated outflow experiments designed for hydraulic parameter estimation, *Water Resour. Res.*, 34(4), 595–602, 1998.
- Hopmans, J. W., and J. Šimůnek, Review of inverse estimation of soil hydraulic properties, in *Proceedings of the International Workshop on Characterization and Measurement of the Hydraulic Properties of Unsaturated Porous Media*, Riverside, CA, 1997, edited by M. T. van Genuchten, F. J. Leij, and L. Wu, pp. 643–659, Univ. of Calif., Riverside, 1999.
- Hopmans, J. W., T. Vogel, and P. D. Koblik, X-ray tomography of soil water distribution in one-step outflow experiments, *Soil Sci. Soc. Am. J.*, 56, 355–362, 1992.
- Kasteel, R., I. Forrer, H. Flüßler, and K. Roth, Solute transport estimated by field- and laboratory-determined hydraulic parameters, in *Proceedings of the International Workshop on Characterization and Measurement of the Hydraulic Properties of Unsaturated Porous Media*, Riverside, CA, 1997, edited by M. T. van Genuchten, F. J. Leij, and L. Wu, pp. 1485–1494, Univ. of Calif., Riverside, 1999.
- Klute, A. (Ed.), *Methods of Soil Analysis, Part 1: Physical and Mineralogical Methods*, 2nd ed., in *Agronomy*, vol. 9, Am. Soc. of Agron., Soil Sci. Soc. of Am., Madison, Wisc., 1986.
- Mortensen, A. P., R. J. Glass, and K. Hollenbeck, Visualization of quasi-2D unsaturated flow during dynamic outflow experiments, *Eos Trans. AGU*, 79(45), Fall Meet. Suppl., F368, 1998.
- Stolte, J., J. I. Freijer, W. Bouten, C. Dirksen, J. M. Halbertsma, J. C. van Dam, J. A. van den berg, G. J. Veerman, and J. H. M. Wösten, Comparison of six methods to determine unsaturated soil hydraulic conductivity, *Soil Sci. Soc. Am. J.*, 58, 1596–1603, 1994.
- Tidwell, V. C., and R. J. Glass, X ray and visible light transmission for laboratory measurement of two-dimensional saturation fields in thin-slab systems, *Water Resour. Res.*, 30(11), 2873–2882, 1994.
- van Dam, J. C., J. N. M. Stricker, and P. Droogers, Inverse method to determine soil hydraulic functions from multistep outflow experiments, *Soil Sci. Soc. Am. J.*, 58, 647–652, 1994.
- Wilkinson, D., Percolation model of immiscible displacement in the presence of buoyancy forces, *Phys. Rev. A*, 30(1), 520–531, 1984.
- R. J. Glass, Flow Visualization and Flow Processes Laboratory, Sandia National Laboratories, P.O. Box 5800, MS 1324, Albuquerque, NM 87185–1324.
- K. Hollenbeck, DHI Water and Environment, Algern Allé 11, DK-2970 Hørsholm, Denmark.
- K. H. Jensen and A. P. Mortensen, Department of Hydrodynamics and Water Resources, Technical University of Denmark, Building 115, DK-2800 Lyngby, Denmark. (annette@isva.dtu.dk)

(Received January 24, 2000; revised December 22, 2000; accepted December 26, 2000.)